Focusing dual-wavelength surface plasmons to the same focal plane by a far-field plasmonic lens

Priyamvada Venugopalan[1], Qiming Zhang[1], Xiangping Li[1], L. Kuipers[3] and Min Gu[1,2*]

[1]Centre for Micro-Photonics, Faculty of Science, Engineering and Technology,
Swinburne University of Technology, Hawthorn, Victoria 3122, Australia
[2]CUDOS and Centre for Micro-Photonics, Faculty of Science, Engineering and Technology,
Swinburne University of Technology, Hawthorn, Victoria 3122, Australia
[3]Centre for Nanophotonics, FOM Institute AMOLF, Science Park 104, 1098 XG Amsterdam, The Netherlands
*Corresponding author: mgu@swin.edu.au

In this work, we demonstrate the nanoscale focusing of surface plasmons at two different wavelengths to the same focal plane by a far-field plasmonic lens both numerically and experimentally. The far-field plasmonic lens, consisting of an annular slit and a concentric groove, capable of focusing dual-wavelength surface plasmons to the same focal plane is characterized by a scanning near-field optical microscope under both linearly and radially polarized illuminations. The demonstrated far-field plasmonic lens can provide immense opportunities for on-chip photonic applications including dual-wavelength based super-resolution imaging and ultra-high density optical data storage.© 2014 Optical Society of America

OCIS Codes: (240.6680) Surface plasmons; (240.0310) Thin films; (180.4243) Microscopy.

Plasmonic focusing devices utilizing the sub-wavelength light confinement and the strong field enhancement of surface plasmons, can break the diffraction limit and allow for the manipulation of light on the sub-wavelength scale, opening up intriguing applications in imaging [1], sensing [2] and integrated optical circuits [3]. As such, plasmonic lenses capable of exciting and focusing surface plasmons (SPs) such as nano hole arrays [4], nano slits [5, 6] and annular ring structures [7, 8] have attracted intense research efforts, although their applications are limited to near-field operations. On the other hand, a plasmonic lens with an annular slit and a concentric groove has been numerically introduced to achieve sub-wavelength focusing at the far-field [9]. Similarly, diffraction limited far-field focusing can be achieved by flat metamaterial based lenses [10]. However, the dispersion of the SPs depends strongly on their frequency and the geometry of the structure. Once the geometry is given, these far-field plasmonic lenses can operate only at a specific wavelength of SPs [11]. Therefore, achieving far-field focusing of multiple wavelengths to the same focal plane remains elusive.

In this work, we present a far-field plasmonic lens capable of focusing of dual-wavelength of light to the same focal plane by optimizing the concentric groove structures. A scanning near-field optical microscopic (SNOM) fibre probe is used to experimentally characterize the focusing properties of the plasmonic lens under both linearly and radially polarized illuminations. The dual-wavelength focusing to the same focal plane is crucial for applications such as stimulated emission depletion based imaging and lithography.

The principle of dual-wavelength focusing by the far-field plasmonic lens, consisting of an annular slit and a concentric groove, is shown in Fig. 1(a). For the realization of far-field focusing of two wavelengths, the groove is placed where the node positions [9, 12] of the two interference patterns of standing waves of SPs match (shown as the dashed square box in the inset of Fig. 1(a)), which scatters the dual-wavelength SPs to the same focal plane. The scattering of the highly confined surface waves into propagating waves is schematically illustrated by the arrows in Fig. 1(a). One example of the designed far-field plasmonic lens is shown in Fig. 1(b). An annular slit structure with a diameter of 5 μm, which is numerically optimized using COMSOL [9], was fabricated by the focused ion beam (FIB) milling method (IonLiNE, Raith) on an Au film of 200 nm thickness, which is deposited on a glass substrate. The depth and width of the annular slit are 200 nm and 350 nm, respectively. The sub-wavelength annular slit acts as a circular grating, couples the incident light into SPs, which gains extra momentum in the direction along the film [13]. The excited SPs can interfere and produce a standing wave pattern while they are propagating towards the center of the lens. Inside the annular slit, a concentric groove is milled with a depth of 80 nm and a width of 100 nm. The inside groove can scatter the SPs out of the interface. The scattered field undergoes interference with the transmitted light from the annular slit, concentrating most of the energy in the far-field regime of the structure. The focus forming efficiency of the structure is calculated around 13% by the simulation.

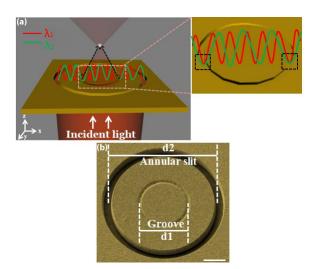In the numerical study through COMSOL, incident beams at the wavelengths of 632.8 nm (λ_1)

Figure 1: (a) Schematic illustration of the principle of a dual-wavelength far-field plasmonic lens (Black single headed arrow lines indicate the scattering of surface waves by the concentric groove). The inset shows the principle of the dispersion control by matching the node position (shown as dashed square boxes) of the surface waves for the two incident wavelengths. (b) SEM image of the far-field plasmonic lens. Scale bar is 1 μm.

and 750.0 nm (λ_2) were chosen. The complex permittivities of Au corresponding to these wavelengths were taken as -9.7997 + i1.9649 and -16.9170 + i1.9602, respectively [14]. The corresponding wavelengths of SPs (λ_{SP}) to these incident wavelengths are 599.0 nm and 727.5 nm, respectively, obtained from Eq. (1)

$$\lambda_{SP} = \lambda_0 \sqrt{\frac{\varepsilon_d + \varepsilon_m}{\varepsilon_d\, \varepsilon_m}} \qquad (1)$$

where, λ_0 is the incident wavelength, ε_d is the dielectric constant of the dielectric substrate and ε_m is the dielectric constant of the metal. Thus, the evanescent standing waves generated at the exit interface of the metal and dielectrics have a variant periodicity as $\lambda_{SP}/2$, following the dispersion of SPs in Eq. (1).

To demonstrate the capability of far-field focusing of the dual-wavelength of light by the plasmonic lens, we first studied the influence of the position of the groove structure at a single incident wavelength of 632.8 nm. The groove was placed at locations where the node of the standing wave pattern appears while keeping its depth and width constant. A high intensity hot spot was observed in the optical axis of the lens, which moves further away from the lens surface, as the groove diameter is increased. Figures 2(a) to (d) show the numerical simulation results of the movement of the hot spot as a function of the groove diameter. Figures 2(e) to (h) show the SEM images of plasmonic lenses with the corresponding groove diameter, d1 of 400 nm, 1000 nm, 1600 nm and 2200 nm, respectively. The efficie-
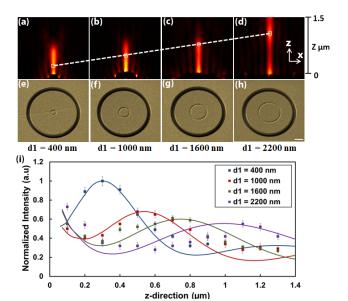

Figure 2: Simulated electric energy distributions (a,b,c,d) and the corresponding SEM images of the far-field plasmonic lens (e,f,g,h) in the vicinity of the far-field plasmonic lens when the groove diameter d1 is 400 nm, 1000 nm, 1600 nm and 2200 nm, respectively. The inclined dashed line in the top figures indicates the shift of the focal length. (i) Comparison between the axial distribution of the normalized transmission intensity of the far-field plasmonic lens obtained by experimental measurements (data points) and simulated results (solid lines). The peaks axially move to larger z-values as the groove diameter increases, indicating the lift of the focal position away with respect to the exit surface of the plasmonic lens or an increased focal length. The wavelength under study is $\lambda_1 = 632.8$ nm.

-ncy of the scattering by the groove is drastically reduced when the groove is moved to the antinode position of the interference pattern of the standing waves. This observation is consistent with a previous report [9].

The simulation of the axial shifting of the focal spot as a function of the groove diameter was corroborated by the SNOM experiment, as shown in Fig. 2(i). To this purpose, the SNOM fibre probe (NT-MDT) with an Aluminium coating of 50 nm in thickness is used for the experimental verification of the influence of the groove structure [15]. The aperture of the probe has a diameter around 50-100 nms which yields a resolution around 100 nm. The transmitted signal from the probe was collected by a single photon photomultiplier tube (PMT). Simulation results of the movement of focal spot away from the lens surface as well as the increase in intensity at the focal plane when the groove position is changed were confirmed by the experimental results. As the focal spot shifts away with respect to the exit surface of the plasmonic lens, the increase in the constructive interference along the axial direction led to an elongated focal spot. Table 1
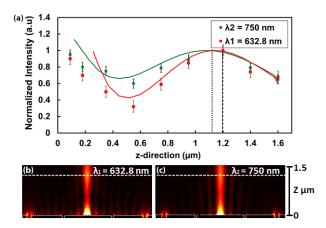
2

Figure 3: (a) Comparison of the axial response of the two incident wavelengths, λ_1 = 632.8 nm and λ_2 = 750 nm (the dotted and dashed lines indicate the focal length of the lens obtained numerically and experimentally). Simulated two-dimensional energy distributions in the xz-plane for (b) λ_1 = 632.8 nm (c) λ_2 = 750 nm (white dashed lines show the focal plane and the white dotted lines show the scheme of the far-field plasmonic lens).

summarizes the lateral full width at half maximum (FWHM) measured from the SNOM images at the focal plane as a function of the groove diameter.

Based on the simulated axial shifting and the lateral confinement of the focal spot at each studied wavelength, the groove radius was optimized at 1100 nm for focusing the dual-wavelength by the far-field plasmonic lens. The dual-wavelength far-field nanofocusing was also experimentally verified by the SNOM probe. A normal Gaussian excitation beam from a broad band laser at the wavelengths of 632.8 nm and 750 nm, respectively was achieved by weakly focusing through an objective lens with a numerical aperture (NA = 0.4) to the far-field plasmonic lens. The beam was collimated at the back aperture of the objective for a uniform excitation of the SPs along the circumference of the structure.

To measure the focal length of the far-field plasmonic lens, a z-scanning method of the fibre probe was employed. The probe was retrieved at regular intervals of 100 nm from the lens surface until it is 2 microns away. At each z-plane, a regular x-y scanning was performed. The axial response of the far-field plasmonic lens was measured for the two incident wavelengths and compared with the focal length given by the numerical simulations. At the optimized groove radius of 1100 nm, corresponding to the node position of SP wavelength of 599.0 nm and 727.5 nm, the plasmonic lens can focus the dual-wavelength SPs to the same focal plane. From the SNOM characterization experiments, the focal length of the far-field plasmonic lens was obtained experimentally as 1.2 µm (dashed lines in Fig. 3(a)), which is identical for both illuminations at the incident wavelengths of
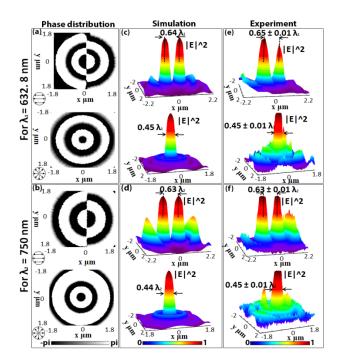

Figure 4: Simulated phase distribution of the longitudinal components in the focal plane of a far-field plasmonic lens under linearly (top panel) and radially (bottom panel) polarized illumination for (a) λ_1 and (b) λ_2. Simulated cross sections of the normalized intensity distributions in the focal region of a far-field plasmonic lens under linearly (top panel) and radially (bottom panel) polarized illumination for (c) λ_1 and (d) λ_2; Experimental cross sections of the normalized intensity distributions in the focal region of a far-field plasmonic lens u nder linearly (top panel) and radially (bottom panel) polarized illumination for (e) λ_1 and (f) λ_2; Polarization orientation is indicated by arrow in the bottom left of each row.

632.8 nm and 750 nm. This result is consistent with the simulation result at 1.15 µm (the dotted lines in Fig. 3(a)). Figures 3(b) and 3(c) show the simulated nanofocusing with the normalized energy distribution in the xz-plane for λ_1 and λ_2, clearly exhibiting focusing to the same far-field focal plane.

In addition, the dual-wavelength far-field plasmonic lens can operate by illuminations at both linear and radial polarization. In the case of the linear polarization excitation, only portions of the annular slit where a component of the incident electric field is perpendicular to the slit edge can excite SPs and this criterion is satisfied only at two opposite points on the circumference of the structure [16]. The E_z components in the focal plane become out of phase (the top panels of Figs. 4(a) and 4(b)) producing two focal lobes in the far-field because of their destructive interference at the center. In the exact focal plane the two-lobe intensity distributions can be obtained for the two incident wavelengths, λ_1 and λ_2.. At the focal plane of 1.2 µm with respect to the lens surface, the separation between the two lobes for λ_1 and λ_2 was measured as 0.65 ± 0.01 λ_1

	d1 = 400 nm		d1 = 1000 nm		d1 = 1600 nm		d1 = 2200 nm	
	Simulation	Experiment	Simulation	Experiment	Simulation	Experiment	Simulation	Experiment
Focal Length (in nms)	370	300 ± 50	635	600 ± 50	880	800 ± 50	1150	1200 ± 50
FWHM of the focal spot	$0.39 \lambda_1$	$0.41 \pm 0.01 \lambda_1$	$0.40 \lambda_1$	$0.41 \pm 0.01 \lambda_1$	$0.42 \lambda_1$	$0.43 \pm 0.01 \lambda_1$	$0.45 \lambda_1$	$0.45 \pm 0.01 \lambda_1$

Table 1: Focusing performance of the far-field plasmonic lens with different groove diameters for an incident wavelength, $\lambda_1 = 632.8$ nm.

and $0.63 \pm 0.01 \lambda_2$ (the top panels of Figs. 4(e) and 4(f)), respectively, which is consistent with the numerical simulations (the top panels of Figs. 4(c) and 4(d)).

For improving the SP excitation efficiency and thereby improving the resolution of the plasmonic lens, a radially polarized illumination was employed. A radial incident polarization, which is always TM (transverse-magnetic) polarized with respect to the outer slit, causes the excitation of SPs all around the slit with their out-of-plane electric field components always in-phase when propagating towards the center [17, 18]. The groove scatters these components to the far-field, producing a much tighter focal spot at the center. This tighter focal spot is attributed to the Ez components being in-phase in the focal plane (the bottom panels of Figs. 4(a) and 4(b)). A single focal spot with much improved resolution was observed numerically in the same focal plane for λ_1 and λ_2 (the bottom panels of Figs. 4(c) and 4(d)). These features were corroborated by the experimental FWHM of the lateral intensity distribution in the focal plane of 1.2 µm, measured as $0.45 \pm 0.01 \lambda_1$ and $0.45 \pm 0.01 \lambda_2$, for the two incident wavelengths respectively (the bottom panels of Figs. 4(e) and 4(f)).

In summary, the nanoscale focusing performance of dual-wavelength SPs to the same focal plane by a far-field plasmonic lens has been demonstrated. This feature is achieved by optimizing the concentric groove structures for the dispersion control of dual-wavelength of SPs and hence demonstrating tunability in the focal length. The dual-wavelength focusing can be operated at both linearly and radially polarized illuminations. The demonstrated far-field plasmonic lens, with an improved resolution compared to its counter parts like microlens arrays [19], may find potential applications in multi-color super-resolution nano lithography [20], stimulated emission depletion imaging systems [21] and ultra-high density optical data storage [22, 23].

References

1. N. Fang, H. Lee, C. Sun, and X. Zhang, Science **308**, 534-537 (2005).
2. S. Lal, S. Link, and N. J. Halas, Nat Photon **1**, 641-648 (2007).
3. E. Ozbay, Science **311**, 189-193 (2006).
4. F. M. Huang, N. Zheludev, Y. Chen, and F. Javier Garcia de Abajo, Appl. Phys. Lett. **90**, 091119 (2007).
5. L. Verslegers, P. B. Catrysse, Z. Yu, J. S. White, E. S. Barnard, M. L. Brongersma, and S. Fan, Nano Lett. **9**, 235-238 (2008).
6. S. Ishii, A. V. Kildishev, V. M. Shalaev, K.-P. Chen, and V. P. Drachev, Opt. Lett. **36**, 451-453 (2011).
7. L. Yin, V. K. Vlasko-Vlasov, J. Pearson, J. M. Hiller, J. Hua, U. Welp, D. E. Brown, and C. W. Kimball, Nano Lett. **5**, 1399-1402 (2005).
8. W. Chen, D. C. Abeysinghe, R. L. Nelson, and Q. Zhan, Nano Lett. **9**, 4320-4325 (2009).
9. M. Zhang, J. Du, H. Shi, S. Yin, L. Xia, B. Jia, M. Gu, and C. Du, Opt. Exp. **18**, 14664-14670 (2010).
10. F. Aieta, P. Genevet, M. A. Kats, N. Yu, R. Blanchard, Z. Gaburro, and F. Capasso, Nano Lett. **12**, 4932-4936 (2012).
11. P. Wróbel, J. Pniewski, T. J. Antosiewicz, and T. Szoplik, Phys. Rev. Lett. **102**, 183902 (2009).
12. A. Y. Nikitin, F. López-Tejeira, and L. Martín-Moreno, Phys. Rev. B **75**, 035129 (2007).
13. M. Mansuripur, A. R. Zakharian, A. Lesuffleur, S.-H. Oh, R. J. Jones, N. C. Lindquist, H. Im, A. Kobyakov, and J. V. Moloney, Opt. Exp. **17**, 14001-14014 (2009).
14. P. G. Etchegoin, E. C. Le Ru, and M. Meyer, J Chem. Phys. **125**, 164705 (2006).
15. P. Venugopalan, Q. Zhang, X. Li, and M. Gu, Opt. Exp. **21**, 15247-15252 (2013).
16. Z. Liu, J. M. Steele, W. Srituravanich, Y. Pikus, C. Sun, and X. Zhang, Nano Lett. **5**, 1726-1729 (2005).
17. Q. Zhan, Opt. Lett. **31**, 1726-1728 (2006).
18. R. Dorn, S. Quabis, and G. Leuchs, Phys. Rev. Lett. **91**, 233901 (2003).
19. Y. Aoki, Y. Shimada, and K. Iga, Japanese J. Appl. Phy. **40**, L446 (2001).
20. Z. Gan, Y. Cao, R. A. Evans, and M. Gu, Nat Commun **4**, 2061 (2013).
21. M. Gu, H. Kang, and X. Li, Sci. Rep. **4**, 3621 (2014).
22. X. Li, J. W. M. Chon, S. Wu, R. A. Evans, and M. Gu, Opt. Lett. **32**, 277-279 (2007).
23. X. Li, T.-H. Lan, C.-H. Tien, and M. Gu, Nat Commun **3**, 998 (2012).

References

1. N. Fang, H. Lee, C. Sun, and X. Zhang, "Sub☐Diffraction-Limited Optical Imaging with a Silver Superlens," Science **308**, 534-537 (2005).

2. S. Lal, S. Link, and N. J. Halas, "Nano-optics from sensing to waveguiding," Nat Photon **1**, 641-648 (2007).

3. E. Ozbay, "Plasmonics: Merging Photonics and Electronics at Nanoscale Dimensions," Science **311**, 189-193 (2006).

4. F. M. Huang, N. Zheludev, Y. Chen, and F. Javier Garcia de Abajo, "Focusing of light by a nanohole array," Appl. Phys. Lett. **90**, 091119 (2007).

5. L. Verslegers, P. B. Catrysse, Z. Yu, J. S. White, E. S. Barnard, M. L. Brongersma, and S. Fan, "Planar Lenses Based on Nanoscale Slit Arrays in a Metallic Film," Nano Lett. **9**, 235-238 (2008).

6. S. Ishii, A. V. Kildishev, V. M. Shalaev, K.-P. Chen, and V. P. Drachev, "Metal nanoslit lenses with polarization-selective design," Opt. Lett. **36**, 451-453 (2011).

7. L. Yin, V. K. Vlasko-Vlasov, J. Pearson, J. M. Hiller, J. Hua, U. Welp, D. E. Brown, and C. W. Kimball, "Subwavelength Focusing and Guiding of Surface Plasmons," Nano Lett. **5**, 1399-1402 (2005).

8. W. Chen, D. C. Abeysinghe, R. L. Nelson, and Q. Zhan, "Plasmonic Lens Made of Multiple Concentric Metallic Rings under Radially Polarized Illumination," Nano Lett. **9**, 4320-4325 (2009).

9. M. Zhang, J. Du, H. Shi, S. Yin, L. Xia, B. Jia, M. Gu, and C. Du, "Three-dimensional nanoscale far-field focusing of radially polarized light by scattering the SPPs with an annular groove," Opt. Exp. **18**, 14664-14670 (2010).

10. F. Aieta, P. Genevet, M. A. Kats, N. Yu, R. Blanchard, Z. Gaburro, and F. Capasso, "Aberration-Free Ultrathin Flat Lenses and Axicons at Telecom Wavelengths Based on Plasmonic Metasurfaces," Nano Lett. **12**, 4932-4936 (2012).

11. P. Wróbel, J. Pniewski, T. J. Antosiewicz, and T. Szoplik, "Focusing Radially Polarized Light by a Concentrically Corrugated Silver Film without a Hole," Phys. Rev. Lett. **102**, 183902 (2009).

12. A. Y. Nikitin, F. López-Tejeira, and L. Martín-Moreno, "Scattering of surface plasmon polaritons by one-dimensional inhomogeneities," Phys. Rev. B **75**, 035129 (2007).

13. M. Mansuripur, A. R. Zakharian, A. Lesuffleur, S.-H. Oh, R. J. Jones, N. C. Lindquist, H. Im, A. Kobyakov, and J. V. Moloney, "Plasmonic nano-structures for optical data storage," Opt. Exp. **17**, 14001-14014 (2009).

14. P. G. Etchegoin, E. C. Le Ru, and M. Meyer, "An analytic model for the optical properties of gold," J. Chem. Phys. **125**, 164705 (2006).

15. P. Venugopalan, Q. Zhang, X. Li, and M. Gu, "Polarization-sensitive characterization of the propagating plasmonic modes in silver nanowire waveguide on a glass substrate with a scanning near-field optical microscope," Opt. Exp. **21**, 15247-15252 (2013).

16. Z. Liu, J. M. Steele, W. Srituravanich, Y. Pikus, C. Sun, and X. Zhang, "Focusing Surface Plasmons with a Plasmonic Lens," Nano Lett. **5**, 1726-1729 (2005).

17. Q. Zhan, "Evanescent Bessel beam generation via surface plasmon resonance excitation by a radially polarized beam," Opt. Lett. **31**, 1726-1728 (2006).

18. R. Dorn, S. Quabis, and G. Leuchs, "Sharper Focus for a Radially Polarized Light Beam," Phys. Rev. Lett. **91**, 233901 (2003).

19. Y. Aoki, Y. Shimada, and K. Iga, "Evaluation of Numerical Aperture and Focusing Characteristics of Planar Microlens for Optical Interconnects," Japanese J. Appl. Phys. **40**, L446 (2001).

20. Z. Gan, Y. Cao, R. A. Evans, and M. Gu, "Three-dimensional deep sub-diffraction optical beam lithography with 9 nm feature size," Nat Commun **4** 2061 (2013).

21. M. Gu, H. Kang, and X. Li, "Breaking the diffraction-limited resolution barrier in fiber-optical two-photon fluorescence endoscopy by an azimuthally-polarized beam," Sci. Rep. **4,** 3621 (2014).

22. X. Li, J. W. M. Chon, S. Wu, R. A. Evans, and M. Gu, "Rewritable polarization-encoded multilayer data storage in 2,5-dimethyl-4-(p-nitrophenylazo)anisole doped polymer," Opt. Lett. **32**, 277-279 (2007).

23. X. Li, T.-H. Lan, C.-H. Tien, and M. Gu, "Three-dimensional orientation-unlimited polarization encryption by a single optically configured vectorial beam," Nat Commun **3**, 998 (2012).